ACS NANO

www.acsnano.org

ARTICLE

Treatment of Acute Liver Injury through Selective Tropism of *High Mobility Group Box 1* Gene-Silenced Large Peritoneal Macrophages

Dhaval Oza, Fernando Ivich, Kirsten Deprey, Kelsey Bittner, Keith Bailey, Sarah Goldman, Mikyung Yu, Mark Niedre, Ho-Chou Tu, and Mansoor M. Amiji*

Cite This: *ACS Nano* 2025, 19, 12102−12118

Read Online

ACCESS | Metrics & More | Article Recommendations | Supporting Information

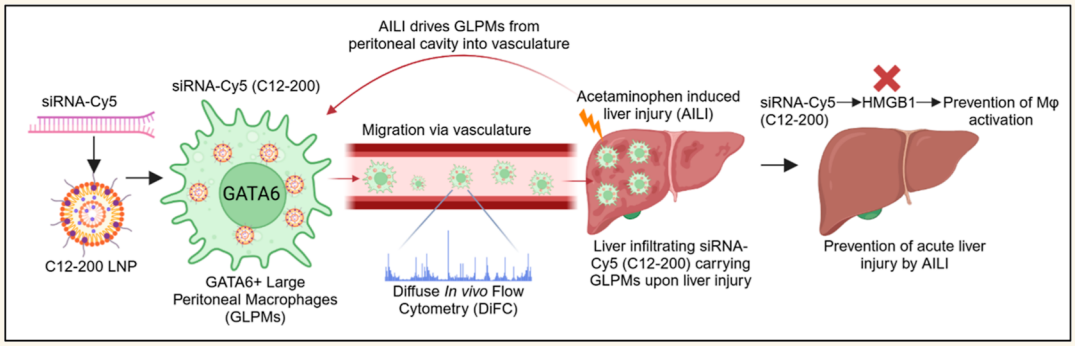

ABSTRACT: **Tissue-resident macrophages (TRMs) are attractive cells to therapeutically deliver oligonucleotide and other gene-expression modifying modalities to treat a wide array of diseases ranging from inflammatory to autoimmune, and even cancer. Here, we focus on TRMs located inside the peritoneal cavity lining the abdomen that selectively express a transcription factor GATA6 called large peritoneal macrophages (GLPMs) and successfully demonstrate functional GLPM-selective delivery of a Cy5-fluorophore-labeled siRNA encapsulated in C12−200 cationic-lipidoid-based nanoparticles (siRNA-Cy5 (C12−200)). Despite being TRMs, GLPMs possess a specific migratory ability to peritoneally located liver tissue upon injury incited by acetaminophen (APAP) overdose in mice. A rapid, liver injury-driven tropism of GLPMs carrying siRNA-Cy5 (C12−200) was seen via systemic circulation, which was elegantly demonstrated by using a noninvasive live-cell tracking technique called diffuse *in vivo* flow cytometry (DiFC). Finally, RNAi-mediated silencing of a well-known pro-inflammatory damage-associated molecular pattern (DAMP) *High Mobility Group Box-1* (HMGB1) gene in GLPMs led to the mitigation of liver injury and inflammation via prevention of GLPM modulation to a pro-inflammatory state, which further translated into significant protection from APAP-driven liver injury and a reduction in liver circulating pro-inflammatory cytokines owing to a muted inflammatory response to acute liver injury. Moreover, silencing HMGB1 by a GalNAc-conjugated hepatocyte-targeting siRNA did not reciprocate the findings, further solidifying our results. Together, our data suggested that GLPMs act as delivery carriers by rapidly bringing lipid nanoparticle-encapsulated RNAi modalities to the injured liver and have emerged as a therapeutically viable strategy to address inflammatory diseases, especially those that are more acute in nature.**

KEYWORDS: *GATA6-expressing large peritoneal macrophages, High Mobility Group Box-1, small interfering RNAs, lipid nanoparticles, acute liver injury, diffuse in vivo flow cytometry*

Tissue-resident macrophages (TRMs) have been at the forefront of immune cell research as well as therapeutic targets for a range of metabolic, inflammatory, autoimmune, and immune-oncology indications.[1,2] Among these TRMs are GATA6+ large peritoneal macrophages (GLPMs) residing in the peritoneal cavity, which present as fascinating cell types to explore for their unique potential to influence immunity and

Received: December 18, 2024
Revised: March 7, 2025
Accepted: March 10, 2025
Published: March 18, 2025

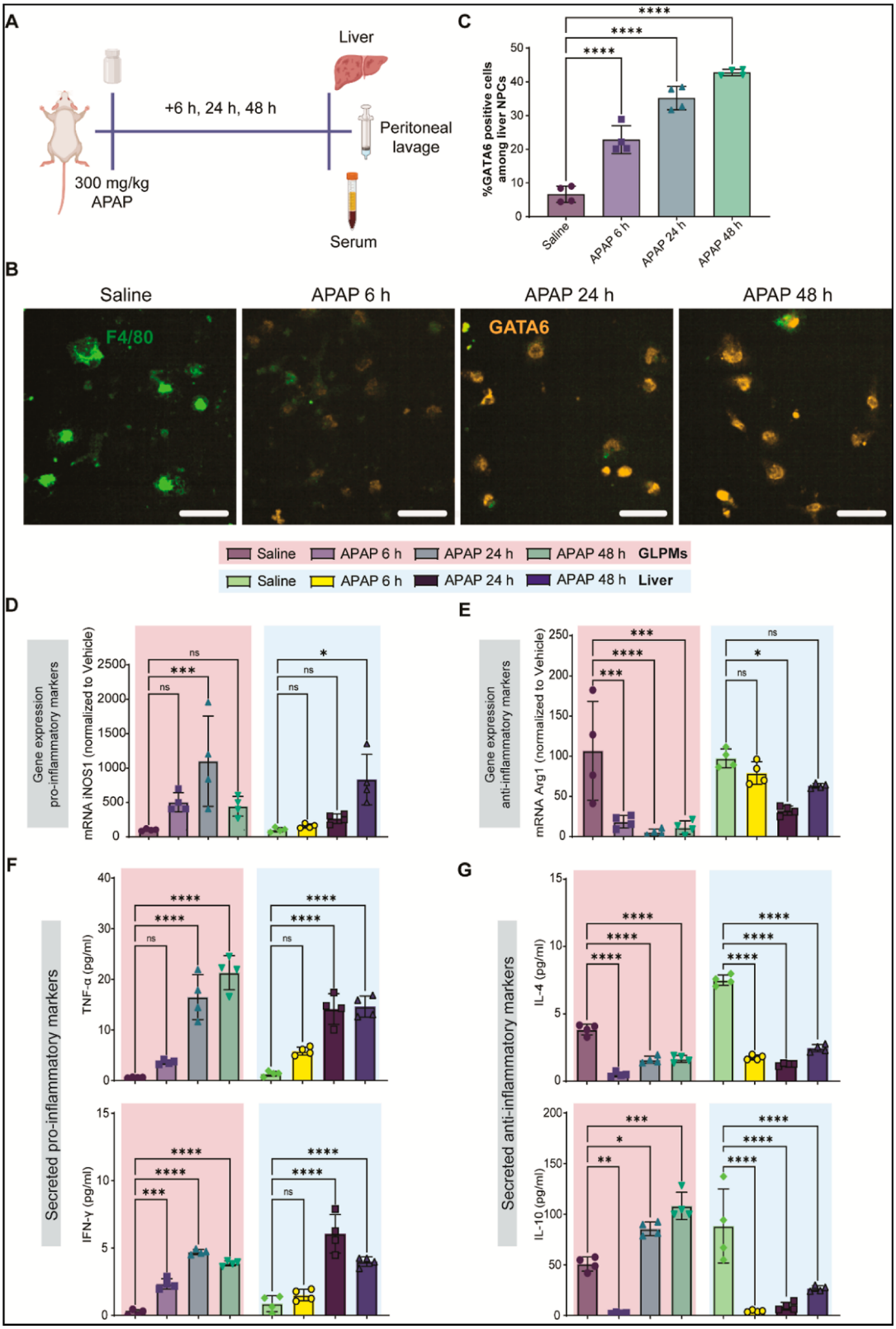

Figure 1. GLPMs migrate to the liver and are driven into a pro-inflammatory state by acute liver injury incited by APAP. (A) Study schematics. (B) Representative IF images of TRM marker F4/80 (green) and GLPM-specific marker GATA6 (yellow) from liver NPCs at 6, 24, and 48 h post intraperitoneal administration of APAP. Saline-treated control mice were treated for 6 h. Scale bars, 100 μm. (C) Quantification of percentage GATA6-expressing cells within the isolated liver NPCs in all the treatment groups. (D) Relative mRNA expression of iNOS1 and (E) Arg1 relative expression in saline control groups. The mRNA expression was derived from quantitative polymerase chain reaction (qPCR) after normalizing the expression with an average of housekeeping genes PPIA and GAPDH. (F) Secreted pro-inflammatory cytokine levels of TNF-α and IFN-γ in pg/mL. (G) Secreted anti-inflammatory cytokine levels of IL-4 and IL-10 in pg/mL. n = 4 for all groups. Data have been

https://doi.org/10.1021/acsnano.4c18345
ACS Nano 2025, 19, 12102−12118

Figure 1. continued

represented as mean ± SD. *$p < 0.05$, **$p < 0.01$, ***$p < 0.001$, ****$p < 0.0001$, ns not significant. *P* values were calculated with an ordinary one-way ANOVA followed by Dunnett's multiple comparison test, with a single pooled variance.

inflammation in surrounding as well as distantly located tissues.[3,4] These cells comprise 80% of all macrophages in the mammalian peritoneum and express a zinc-finger transcription factor, GATA6, which is not only important for their development and survival but is also selectively expressed in these "cavity-resident" macrophages among all myeloid cells across all tissues.[5,6] GLPMs have evolutionarily conserved roles, forming a protective barrier of highly conserved cavity-resident macrophages stemming from over 500 million years of evolution, and have their origins in embryogenic precursors just like other TRMs.[5,7] What makes them special is that although they have been categorized as tissue-resident, they are not necessarily resident within any tissue in a normal physiological state and can migrate and contribute to immunological responses in surrounding abdominal tissues like liver and intestines or the surrounding omentum.[4,8,9] Recent evidence also points out their migratory ability to tissues outside the peritoneum like lungs in a pathophysiological setting, making them a unique readily available mature macrophage population vital for orchestrating an immune response in various tissues.[10]

Although macrophages, including TRMs, are vital therapeutic targets considering a range of roles that they carry out, the lack of a functional cell-selective delivery with many nucleic acid therapies and the complexity of vastly nuanced and different macrophage phenotypic states make them a difficult cell type to target and modulate.[1,2,11−13] Our findings revealed that the migratory ability of GLPMs to neighboring injured tissues can also be seen in a more physiologically relevant model of drug-induced acute liver injury (ALI) incited by acetaminophen (APAP) overdose in mice.[14] Along with that, we demonstrated a rapid intravasation of GLPMs using a novel live cell tracking technique called diffuse *in vivo* flow cytometry (DiFC) and further confirmed that liver infiltration of GLPMs was completely dependent on liver injury.[15−18] Furthermore, we demonstrate a clinically translatable application of this migratory property by delivering an siRNA using a GLPM-selective C12-200-based lipid nanoparticle (LNP) delivery system which was previously validated to deliver siRNAs selectively to GLPMs.[10] The compound C12-200 is a polycationic lipidoid that has a piperazine ring with 5 amino alcohol lipid tails. C12-200 lipidoid has been known to exhibit approximately 100 times more efficiency than earlier lipidoid-like carriers and has been previously characterized as having extensive siRNA-mediated gene-silencing ability in myeloid cells.[19−21] We picked a High Mobility Group-Box 1 (HMGB1) protein to therapeutically silence by siRNAs to mitigate APAP-induced inflammation. HMGB1 is a well-known nuclear protein, which can serve as one of the key pro-inflammatory cytokines when released.[22] Its translocation from the nuclei to the cytoplasm and eventual secretion is one of the important events in sterile inflammation, and it acts as one of the major damage-associated molecular patterns (DAMPs).[23−25] Extracellularly, among its interactions with various receptors, primarily it can activate toll-like receptors (TLR) and receptors for advanced glycation end products (RAGE) to stimulate immune cells and amplify sterile injury.[23−25] By silencing *HMGB1* gene within GLPMs, we were able to prevent liver injury and inflammation by blocking pro-inflammatory macrophage activation, which in turn influenced the injured liver microenvironment in muting the inflammatory response downstream to hepatocyte-necrosis triggered by APAP-hepatotoxicity.[26,27]

In terms of the clinical meaningfulness of acetaminophen-induced liver injury (AILI), AILI by drug overdose, although relatively rare, is often fatal, and has led to a significant increase in incidences of liver failure and with it, an increase in the need for liver transplants.[28,29] Hence, our work not only highlights a seemingly inherent and fundamentally conserved property of a unique type of TRM, but by achieving functional RNAi delivery to these cells, it also demonstrates a potential clinical benefit of delivering an RNAi-therapeutic to GLPMs and using them as delivery carriers to also address acute injuries and inflammatory conditions like AILI.

RESULTS

GLPMs Migrate to the Liver in the APAP-Induced Acute Liver Injury Model. GLPMs selectively express transcription factor GATA6, which is expressed neither by liver resident Kupffer cells nor by circulating monocytes and hence is a promising GLPM-specific marker by which we intended to probe for infiltrating GLPMs to the liver after AILI. Female BALB/c mice were intraperitoneally administered a 300 mg/kg dose of APAP for 6, 24, and 48 h. Significant upregulation of circulating liver injury enzymes as well as an increase in total bilirubin levels confirmed liver injury incited by APAP (Figure S1A). Histopathological evaluation revealed widespread acute central coagulative necrosis by 6 h, confirming an acute injury phenotype, followed by infiltration of liver infiltrating immune cells within 24−48 h (Figure S1B).

Immunofluorescence (IF) staining of GATA6 from isolated liver nonparenchymal cells (NPCs) demonstrated a clear costaining of GATA6 with mouse macrophage marker F4/80, revealing a significant infiltration of GLPMs into the liver at all the measured time points post AILI (6, 24, and 48 h) (Figure 1B). Overall, there was a clear increase in GLPM infiltration to the liver from 6 to 48 h, as also confirmed by liver IHC (Figures 1C and S1C).

AILI Drives GLPMs into a Pro-inflammatory State. There was a significant increase in the relative gene expression of classic macrophage pro-inflammatory markers like inducible nitric oxide synthase-1 (iNOS1) in not only the liver but also the GLPM population, with the most significant increase seen by 24 h in the GLPMs. Meanwhile in the liver, there was an increasing trend from 6 to 48 h (Figure 1D). Along with this, expression of classic anti-inflammatory marker arginase-1 (Arg1) was significantly reduced in GLPMs (Figure 1E). Along with this, there was a significant increase in some secreted pro-inflammatory cytokines in GLPMs like tumor necrosis factor-alpha (TNF-α) and interferon-gamma (IFN-γ) as well as a reduction in other anti-inflammatory cytokines like interleukin-4 (IL-4) (Figure 1F,G) that was measured in the peritoneal lavage supernatant. Additionally, many other measured putative pro-inflammatory circulating cytokines were upregulated in both peritoneal lavage supernatant and liver NPCs by 6 h, many of which were further increased by 24 and 48 h post-APAP

https://doi.org/10.1021/acsnano.4c18345
ACS Nano 2025, 19, 12102−12118

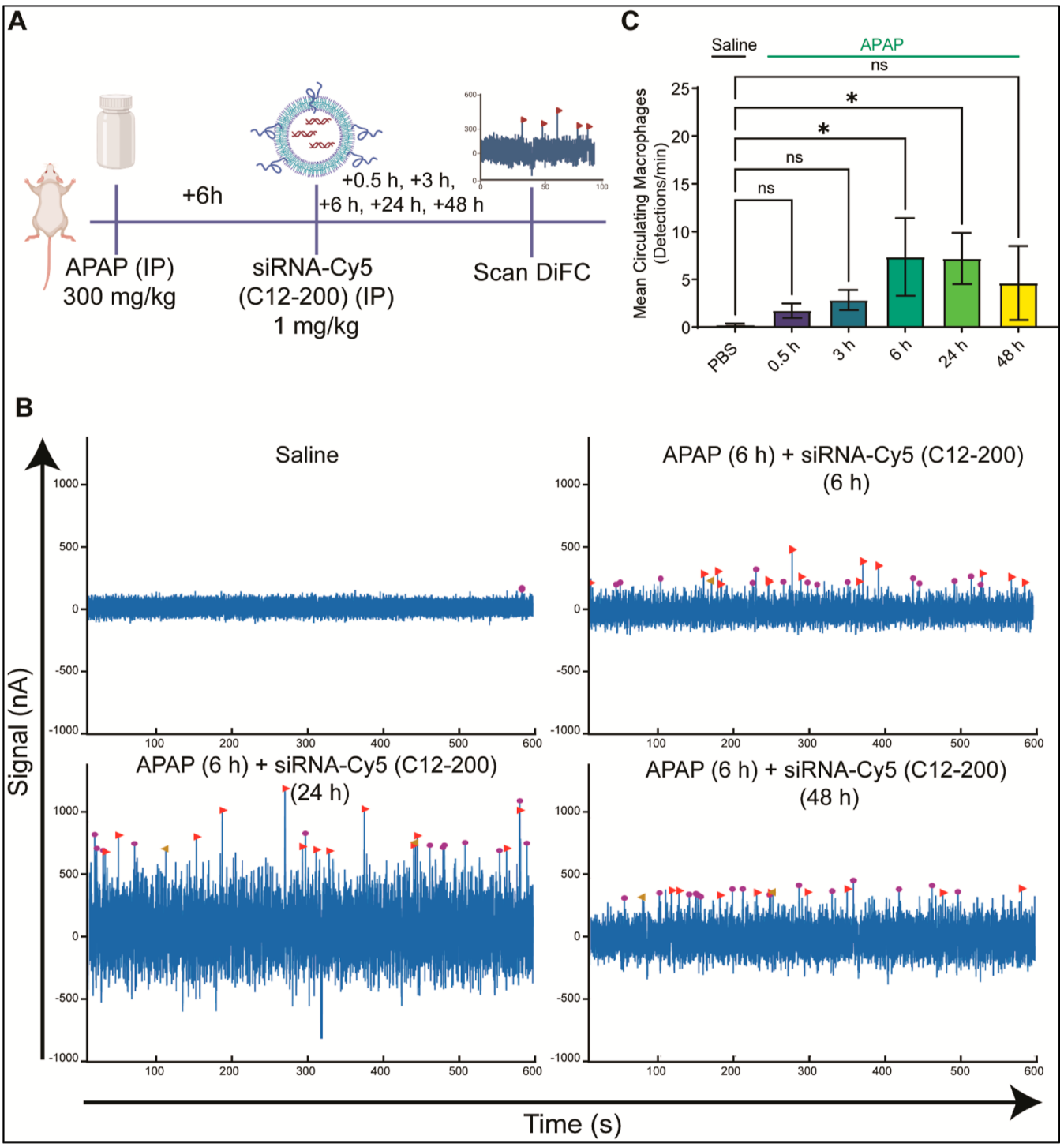

Figure 2. Systemically circulating siRNA-Cy5 (C12−200)-labeled GLPMs are detected by DiFC upon APAP-induced acute liver injury. (A) Study schematics of DiFC mouse studies post APAP (6 h) + siRNA-Cy5 (C12-200) administration (0.5, 3, 6, 24, 48 h). Saline (6 h) + PBS (48 h) was used as a control. (B) Representative DiFC scans depicted as number of peaks detected over 600 s from one mouse per group from an $n = 4$/group with the indicated treatments. Graphs are representative snapshots of a 10 min scan period from a single mouse from a total scanning time of 45 min per mouse. The graphs for 0.5 and 3 h are not depicted here; refer to Figure S4 for DiFC graphs for all time points. Each peak (arrowhead) represents a circulating cell labeled with siRNA-Cy5 (C12−200) in systemic circulation, depicted as signal versus time. (C) Quantification of mean circulating macrophages per min as detected by DiFC from a total scan time of 45 min. $n = 4$ for all the treatment groups. Data have been represented as mean ± SD. *$p < 0.05$, **$p < 0.01$, ***$p < 0.001$, ****$p < 0.0001$, ns not significant. P values were calculated with an ordinary one-way ANOVA followed by Dunnett's multiple comparison test, with a single pooled variance.

administration (Figure S2A,B). This suggested that liver injury driven by APAP led to significant changes in the phenotypic state of GLPMs located in the surrounding abdominal cavity, driving them into a pro-inflammatory state.

Systemically Circulating GLPMs Were Detected by DiFC in the AILI Model. For all GLPM-tracking studies, Cy5 fluorophore-labeled siRNAs targeting Gaussia luciferase (control siRNA) were formulated into LNPs utilizing macrophage-

https://doi.org/10.1021/acsnano.4c18345
ACS Nano 2025, 19, 12102−12118

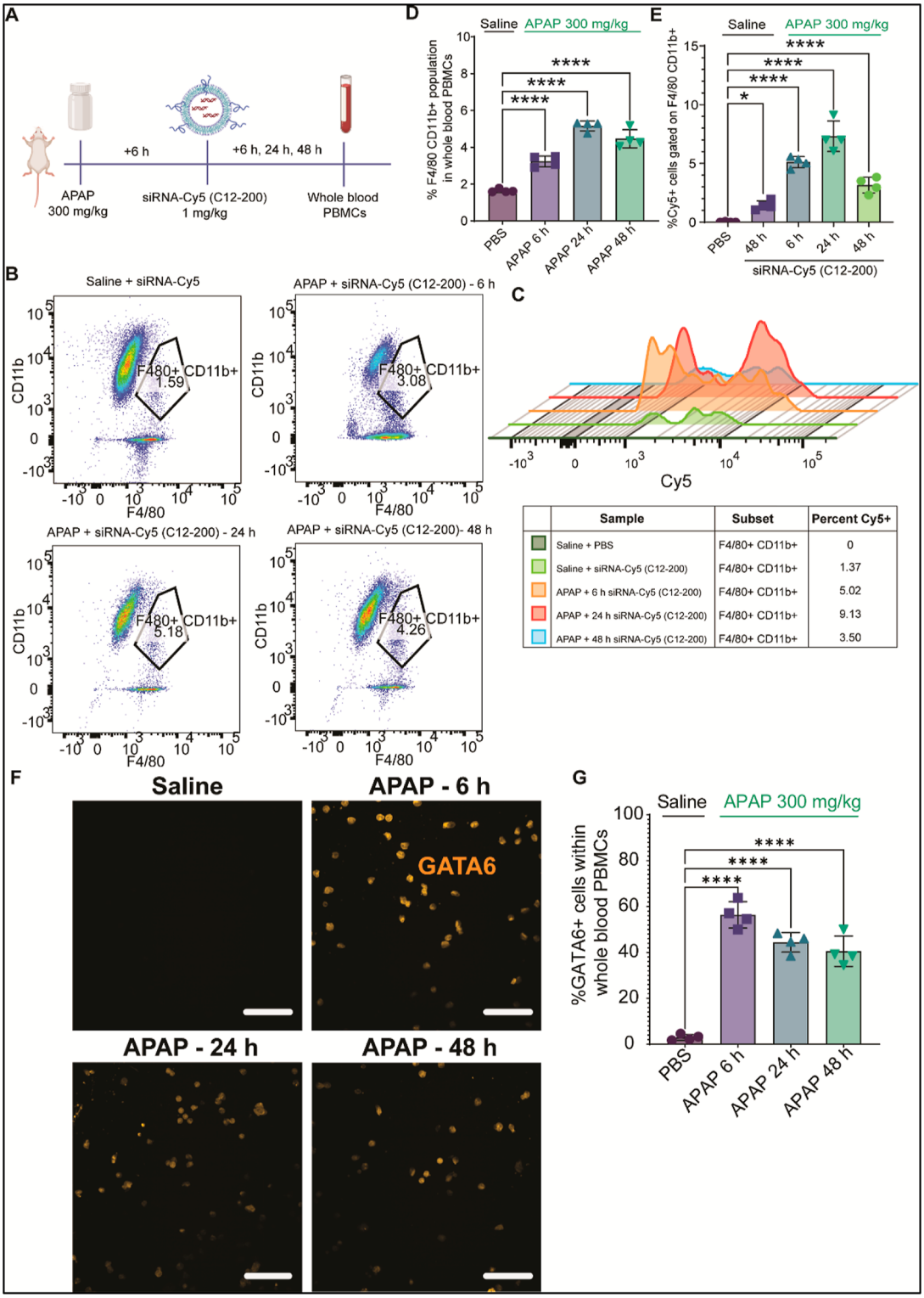

Figure 3. Circulating GLPMs are seen in whole blood PBMCs following acute liver injury by APAP. (A) Study schematics and (B) flow cytometry analysis showing representative dot plots of F4/80$_{hi}$ CD11b$_{hi}$ macrophage population of respective treatment groups in isolated PBMCs. (C) Representative histograms of Cy5+ cells within the F4/80$_{hi}$ CD11b$_{hi}$ macrophage population. Cells were pregated on size and viability. Data are representative of one sample from an n = 4 per treatment group. (D) Quantification of the overall percentage of F4/80$_{hi}$ CD11b$_{hi}$ in whole blood PBMCs with the indicated treatment groups. (E) Quantification of percentage Cy5+ cells within the F4/80$_{hi}$ CD11b$_{hi}$ gated macrophage population with the indicated treatment groups. (F) Representative IF images of GLPM-specific marker GATA6 (yellow) in the isolated whole blood PBMC lymphocytes with the indicated treatment groups. Scale bars, 200 μm. (G) Quantification of percentage GATA6-expressing cells within the isolated whole blood PBMC lymphocytes with the treatment groups. n = 4 for all groups. Data have been represented as mean ± SD. *p < 0.05, **p < 0.01, ***p < 0.001, ****p < 0.0001, ns not significant. P values were calculated with an ordinary one-way ANOVA followed by Dunnett's multiple comparison test, with a single pooled variance.

https://doi.org/10.1021/acsnano.4c18345
ACS Nano 2025, 19, 12102−12118

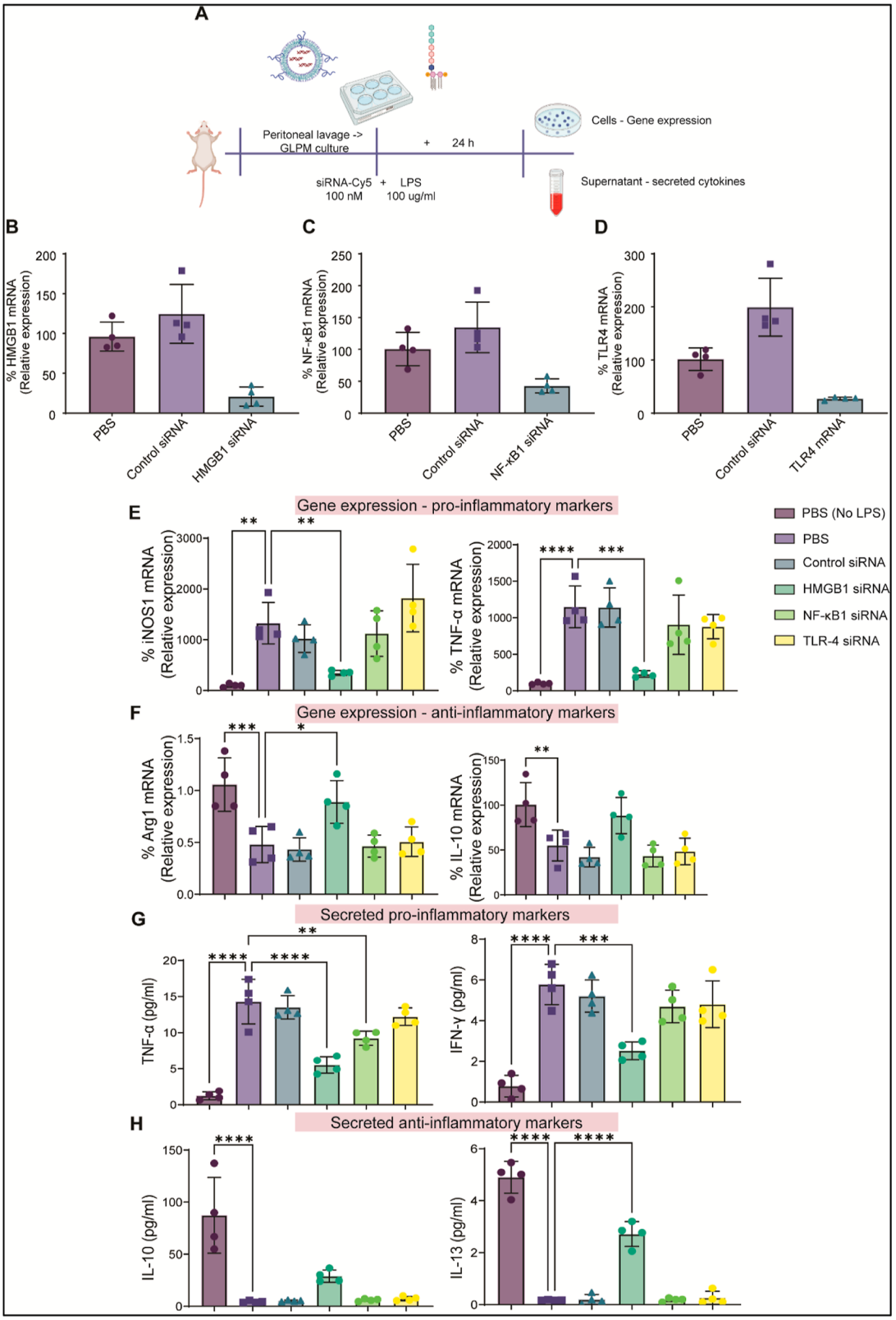

Figure 4. siRNA-mediated *HMGB1* silencing renders protection from inflammation induced by LPS in vitro in GLPMs. (A) Study schematics. (B) Relative mRNA expression of HMGB1, (C) NF-κB1, and (D) TLR-4, depicted as percentage mRNA remaining relative to expression in PBS-treated controls. mRNA expression was derived from qPCR after normalizing expression with an average of housekeeping genes PPIA and GAPDH. (E) Relative mRNA expression of iNOS1 and TNF-α, and (F) Arg1 and IL-10 were relative to expression in saline control groups. (G) Secreted pro-inflammatory cytokine levels of TNF-α and IFN-γ in pg/mL. (H) Secreted anti-inflammatory cytokine levels of IL-4 and IL-10 in pg/mL. $n = 4$ for all groups. Data have been represented as mean ± SD. *$p < 0.05$, **$p < 0.01$, ***$p < 0.001$, ****$p < 0.0001$, ns not significant. *P* values were calculated with an ordinary one-way ANOVA followed by Dunnett's multiple comparison test, with a single pooled variance.

https://doi.org/10.1021/acsnano.4c18345
ACS Nano 2025, 19, 12102−12118

selective C12-200 ionizable lipid as the delivery system owing to its previous characterization of selectively delivering siRNAs into GLPMs.[10] Synthesis and formulation of C12-200-encapsulated siRNA-Cy5 was just as previously described and was accordingly characterized for encapsulation efficiency and siRNA concentration (Table S2).[10]

The ability of GLPMs to intravasate and migrate to nonperitoneally located lungs via systemic circulation upon depleting out the lung-resident AMs has been previously seen.[10] Here, we wanted to expand earlier findings in the context of an acute injury model within peritoneally located liver tissue. So, we tracked these fluorophore-labeled GLPMs within the vasculature utilizing DiFC that was previously used to track the migration of these cells to the lungs from the peritoneal cavity.[10] DiFC is an optical technique that enables the detection of fluorescent cells circulating in the blood of small animals in real-time.[17] The working principle of DiFC has been thoroughly described and used in various mouse models.[15,17,18] Figure S3 depicts DiFC study schematics. In short, DiFC detects a signal spike, or "peak", when a fluorescent cell passes by the instrument's field of view.[16] The validity of the detected peaks has been previously confirmed in phantoms as a reliable tool to detect siRNA-Cy5 (C12−200) labeled GLPMs.[10]

Since we already saw a significant liver infiltration of GLPMs at 6 h (Figure 1), we were keen to probe for circulating siRNA-Cy5 (C12−200)-labeled GLPMs at earlier time points. Hence, 300 mg/kg APAP was intraperitoneally injected for 6 h, followed by 1 mg/kg intraperitoneal administration of the siRNA-Cy5 (C12−200) since 1 mg/kg siRNA (administered in C12−200 LNP) was previously shown to demonstrate selective and robust siRNA uptake into GLPMs.[10] Control mice were dosed with a weight-equivalent dose of 1× PBS. DiFC was performed on live mice, and data were collected at 0.5 3, 6, 24, and 48 h post siRNA-Cy5 (C12−200) administration to look for circulating "peaks" of Cy5-labeled circulating cells (Figure 2A). At every time point, mice were scanned for 45 min in quadruplicate, allowing for counting the labeled macrophages in systemic circulation in real-time post APAP and siRNA-Cy5 (C12-200) injections (Figure S4B). Detection of these transient Cy5 cell "peaks" only upon APAP administration indicated circulating cellular events (Figure 2B). The number of Cy5-labeled cells in circulation appeared to peak between 6 and 24 h post siRNA-Cy5 (C12-200) administration and seemed to be driven by APAP-induced liver-injury (Figure 2B,C).

AILI Leads to Intravasation of GLPMs into Systemic Circulation. Next, we looked for a mature TRM population in whole blood peripheral blood mononuclear cells (PBMCs) by flow cytometry and subsequently carried out IF staining of LPM-specific marker GATA6 following APAP administration to confirm whether liver injury drove some of these peritoneally resident TRMs into the vasculature. APAP was intraperitoneally injected for 6 h at a 300 mg/kg dose along with a saline control. Whole blood PBMCs, when isolated and gated for mature TRM F4/80+ CD11b+ cells at 6 h, 24 and 48 h post siRNA-Cy5 (C12-200) administration, revealed a significant increase in the F4/80+ CD11b+ TRMs circulating in the APAP-administered mice compared to saline-treated mice (Figures S5B and 3B,D). Moreover, the percentage of Cy5+ cells gated within the F4/80+ CD11b+ cell population significantly increased in the PBMCs from APAP-treated mice compared to saline controls, especially at 6 and 24 h, similar to the DiFC Cy5-labeled cellular "peaks" (Figures 2C and 3C,E). Additionally, IF staining of isolated PBMCs to look for GLPM-specific marker GATA6 revealed the presence of nuclear GATA6+ LPMs (Figure 3F), confirmed by overlap with DAPI stain only seen in the APAP-treated groups (Figure S6). This demonstrated that the migration and intravasation of GLPMs into the vasculature were dependent on AILI incited by APAP.

Hence, a rapid liver-injury-driven tropism of peritoneally resident GLPMs along with the presence of these cells in systemic circulation within hours after liver injury raised the possibility of modulating GLPMs to mitigate liver injury by intraperitoneally delivering a therapeutic modality like siRNA via GLPM-selective C12-200-based LNPs.

C12−200 LNPs Were Effective in *In Vitro* Silencing of Pro-inflammatory Genes *HMGB1*, *NB-κB*, and *TLR-4* in Primary Mouse GLPMs. We next sought to characterize RNAi-mediated gene silencing of some well-characterized pro-inflammatory targets within GLPMs and eventually demonstrate whether this could be a meaningful therapy for acute liver injuries. For this purpose, we picked a well-characterized DAMP like High Mobility Group Box-1 (HMGB1) protein, its putative receptor on macrophages toll-like receptor-4 (TLR-4), and finally, the pro-inflammatory transcription factor nuclear factor-κB (NF-κB) as the targets from one of the most well-conserved central nodes of inflammation amplifying genes that we could silence using an siRNA in GLPMs.[26,27,30−32] Chemically modified siRNAs targeting *HMGB1*, *TLR-4*, *NF-κB*, and *gLuc* (control) genes were synthesized as previously described, and their sense strands were labeled with a Cy5 fluorophore (Figure S7A and Table S2).[10,21] Synthesized siRNAs were then formulated into the C12−200-based LNPs (Table S3).[33] Upon transfecting isolated primary mouse GLPMs from peritoneal lavage with 100 nM of the respective siRNA-Cy5 (C12−200) treatments along with an equal volume of 1× PBS control for 24 h, robust mRNA silencing for all the targets was achieved, with an 80%, 70%, and 60% mRNA knockdown (KD) of *HMGB1*, *TLR-4*, and *NF-κB*, respectively, seen when expression was normalized to PBS control (Figure S7C−E). This validated the potency of the tested siRNA sequences. Also, no nonspecific silencing of any of our target genes was seen with the control *gLuc*-targeting siRNA.

siRNA-Mediated *HMGB1* Silencing in GLPMs Renders Protection from Inflammation by LPS *In Vitro*. Next, we utilized the lipopolysaccharide (LPS)-stimulated macrophage activation model as the in vitro model system, which would resemble a pro-inflammatory macrophage phenotype in vivo to validate the inflammation-mitigating ability of RNAi-mediated silencing of HMGB1, TLR4, and NF-κB by measuring pro- and anti-inflammatory macrophage markers post-LPS treatment.[34]

Upon subjecting primary mouse GLPMs to 100 μg/mL LPS dissolved in 1× PBS, *HMGB1* silencing led to the most significant reduction in gene expression of the classic macrophage pro-inflammatory markers iNOS-1 and TNF-α (Figure 4A−E). Also, anti-inflammatory markers Arg1 and IL-10 were not as significantly downregulated in the *HMGB1* siRNA-treated group as the PBS-treated group when compared to the no-LPS control (Figure 4E,F). Along with this, secreted cytokines measured from the cell supernatant also showed a similar trend wherein there was a significant reduction in circulating pro-inflammatory cytokines TNF-α and IFN-γ. Levels of anti-inflammatory markers such as IL-10 and IL-13 did not reduce as much in the *HMGB1* siRNA-treated group as in the PBS-treated group when compared to the no-LPS control (Figure 4G,H). Although *NF-κB* silencing also led to a slight prevention in LPS-induced pro-inflammatory macrophage

https://doi.org/10.1021/acsnano.4c18345
ACS Nano 2025, 19, 12102−12118

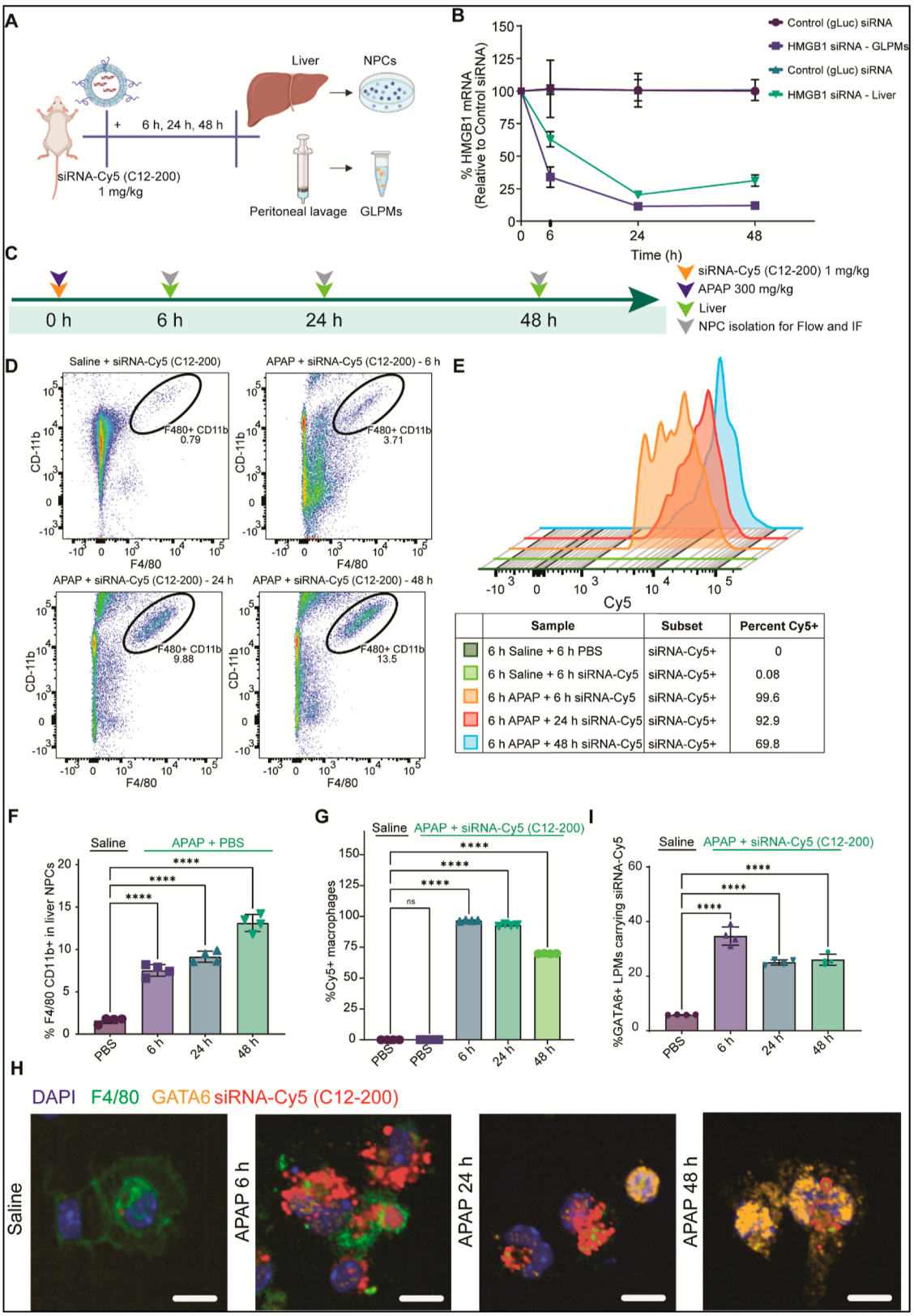

Figure 5. Effective *in vivo* silencing of *HMGB1* gene in GLPMs and rapid migration of siRNA carrying GLPMs to the injured liver post AILI. (A) Study schematics to assess HMGB1 mRNA PD in isolated GLPMs and liver NPCs. (B) Relative mRNA expression of HMGB1 depicted as percentage mRNA remaining relative to expression in gLuc (control) siRNA at 6, 24, and 48 h post-siRNA-Cy5 (C12-200) administration in both GLPMs and liver. The mRNA expression was derived from qPCR after normalizing expression with an average of housekeeping genes PPIA and GAPDH. n = 4 for all groups. (C) Study schematics to look at GLPM carrying siRNA-Cy5 (C12−200) to the liver upon AILI. (D) Flow cytometry analysis showing representative dot plots of F4/80$_{hi}$ CD11b$_{hi}$ macrophage population of respective treatment groups in isolated liver NPCs. (E) Representative histograms of Cy5+ cells within the F4/80$_{hi}$ CD11b$_{hi}$ macrophage population. Cells were pregated on size and viability. Data are representative of one sample from an n = 4 per treatment group. (F) Quantification of the overall percentage of F4/80$_{hi}$

https://doi.org/10.1021/acsnano.4c18345
ACS Nano 2025, 19, 12102−12118

Figure 5. continued

$CD11b_{hi}$ in liver NPCs with the indicated treatment groups. (G) Quantification of percentage Cy5+ cells within the $F4/80_{hi}$ $CD11b_{hi}$ gated macrophage population with the indicated treatment groups. (H) Representative IF images of nuclear staining with DAPI (blue), TRM marker F4/80 (green), GLPM-specific marker GATA6 (yellow), and marker for siRNA-Cy5 (C12-200) (red) from liver NPCs at 6, 24, and 48 h post intraperitoneal administration of APAP. Saline-treated control mice were treated for 6 h. Scale bars, 50 μm. (I) Quantification of percentage siRNA-Cy5 (C12-200) carrying GATA6-expressing cells within the isolated liver NPCs in all the treatment groups. $n = 4$ for all groups. Data have been represented as mean ± SD. *$p < 0.05$, **$p < 0.01$, ***$p < 0.001$, ****$p < 0.0001$, ns not significant. *P* values were calculated with an ordinary one-way ANOVA followed by Dunnett's multiple comparison test, with a single pooled variance.

activation owing to some reduction in pro-inflammatory cytokine TNF-α, silencing of *HMGB1* gene led to a clear prevention of macrophage activation to a pro-inflammatory phenotype by LPS (Figure 4G). Overall, these data suggested that inhibiting a more upstream DAMP like HMGB1 in GLPMs leads to better prevention of LPS-induced macrophage activation and might potentially render protection against acute inflammation and downstream propagation to injury caused by APAP in vivo.

C12-200 LNP Encapsulated siRNA Effectively Silences *HMGB1* in GLPMs *In Vivo*. To assess the *in vivo* pharmacodynamic (PD) properties of the siRNA-Cy5 (C12-200) targeting *HMGB1*, 1 mg/kg of HMGB1 siRNA-Cy5 (C12-200) was dosed intraperitoneally to female BALB/c mice along with a g-Luc control siRNA (Figure 5A) and peritoneal lavage and livers were isolated at 6, 24, and 48 h postinjection. Isolated peritoneal lavage was enriched for GLPMs. Based on the gene expression analysis, there was already a significant mRNA KD of *HMGB1* with the intraperitoneally administered siRNA-Cy5 (C12−200) by 6 h, with only 30% HMGB1 mRNA remaining compared to the gLuc control siRNA where there was no reduction in expression (Figure 5B). KD improved further by 24 h and was sustained to around 90% silencing of HMGB1 until 48 h compared to gLuc control siRNA (Figure 5B).

Along with GLPMs, we also measured PD in isolated liver NPCs since C12-200 LNPs may eventually be taken up by the liver and lead to a functional KD of HMGB1 transcripts within the liver. KD in liver NPCs was minimal at 6 h postinjection, with a more significant KD of 75% seen by 24 h, which was starting to recover by 48 h (Figure 5B). This was an important finding since it showed that intraperitoneally administered siRNA-Cy5 (C12−200) led to an effective KD of target mRNA even at an earlier time point of 6 h in GLPMs but not in the liver.

Hence, these LNPs would become viable to test our hypothesis of mitigating inflammation in the liver post-AILI simply by silencing *HMGB1* in these liver infiltrating GLPMs. Since we established earlier that there was significant infiltration of GLPMs into the liver already at 6 h, upon preventing the release of HMGB1 from these cells within the first 6 h of APAP administration, we could potentially mute the inflammatory response or may even completely prevent the downstream amplification of injury to the liver caused by APAP-induced hepatoxicity.

Selective Tropism of *HMGB1* Silenced GLPMs from the Peritoneal Cavity to the Liver Occurs in AILI. To further confirm liver injury-driven tropism of these *HMGB1*-targeting siRNA-Cy5 (C12-200) encapsulated GLPMs, we again utilized flow cytometry analysis as well as IF staining of GLPM-maker GATA6. After dosing mice with both APAP and siRNA-Cy5 (C12-200), flow cytometry analysis of the harvested NPCs revealed a significant increase in the percentage of mature F4/80+ CD11b+ TRM population (Figure 5C,D,F) (Figure S8). Also, within this F4/80+ CD11b+ population, there was a significant increase in the percentage of Cy5+ cells in the APAP-treated groups at all the time points of 6, 24, and 48 h compared to the saline + siRNA-Cy5 (C12-200) and saline + PBS controls (Figure 5E,G). This suggested liver tropism of siRNA-Cy5 (C12-200) containing GLPM contingent on liver injury incited, especially since there was no Cy5 signal seen in the liver NPCs in the saline (C12-200)-treated group. IF staining of isolated NPCs also revealed a significant increase in the percentage of siRNA-Cy5 (C12-200) carrying-GLPMs at 6, 24, and 48 h when compared to the saline-treated control (Figure 5H,I). Most infiltration was seen at 6 h post-siRNA-Cy5 (C12-200) administration.

Both rapid siRNA-mediated silencing of *HMGB1* in GLPMs and a significant migration of these siRNA-carrying GLPMs to the liver by 6 h suggested this being a viable therapeutic strategy to mitigate acute liver inflammation elicited by APAP.

Additionally, we also evaluated the biosafety profile of the sRNA-Cy5 (C12-200) LNPs by evaluating their in vivo and in vitro immunogenicity profile. Intraperitoneal dosing of PBS and control (gLuc) siRNA-Cy5 (C12-200) dosed at 1 mg/kg for 24 h in WT mice did not lead to any changes in the extensive list of cytokines measured in serum as well as peritoneal lavage (Figure S8).

***HMGB1* Gene Silencing in GLPMs Renders Robust Protection from APAP-Induced Hepatotoxicity.** Simultaneous administration of 1 mg/kg of *HMGB1*-targeting or gLuc (control) siRNAs and 300 mg/kg of APAP was carried out intraperitoneally along with 150 mg/kg of *N*-acetyl cysteine dosed orally (Figure 6A). NAC is a clinically validated antidote for APAP toxicity and is used as a positive control.[35] First, HMGB1 mRNA silencing was confirmed in the GLPMs, with about 70%, 90%, and 90% mRNA silencing observed at 6, 24, and 48 h, respectively, compared to control siRNA (Figure 6B).

Serum liver injury biomarkers such as ALT, AST, and TBil revealed significant protection from liver injury in the HMGB1-treated groups at all the measured time points (Figure 6C). Importantly, there seemed to be a robust response to HMGB1 siRNA treatment by the significantly lower serum ALT, AST, and TBil levels at the early time point of 6 h post HMGB1 treatment, which almost looked trending similarly to the saline-treated group (Figure 6C). As expected, NAC-treatment also led to a significant reduction in the liver injury markers, generally at all the time points (Figure 6C); however, the effect of liver protection seemed smaller than that of the *HMGB1* siRNA-treated group. Liver histopathological evaluation after hematoxylin and eosin (H&E) staining revealed complete protection from hepatocellular degeneration/necrosis at all the measured time-points for mice administered with HMGB1 siRNA compared to gLuc (control) siRNA (mild to moderate) or NAC (minimal to mild) (Figure 6D). Evaluation scores revealed almost complete protection against APAP-induced liver injury in the livers of mice treated with HMGB1 siRNA at all the time points with a significant protection also seen with NAC-

https://doi.org/10.1021/acsnano.4c18345
ACS Nano 2025, 19, 12102−12118

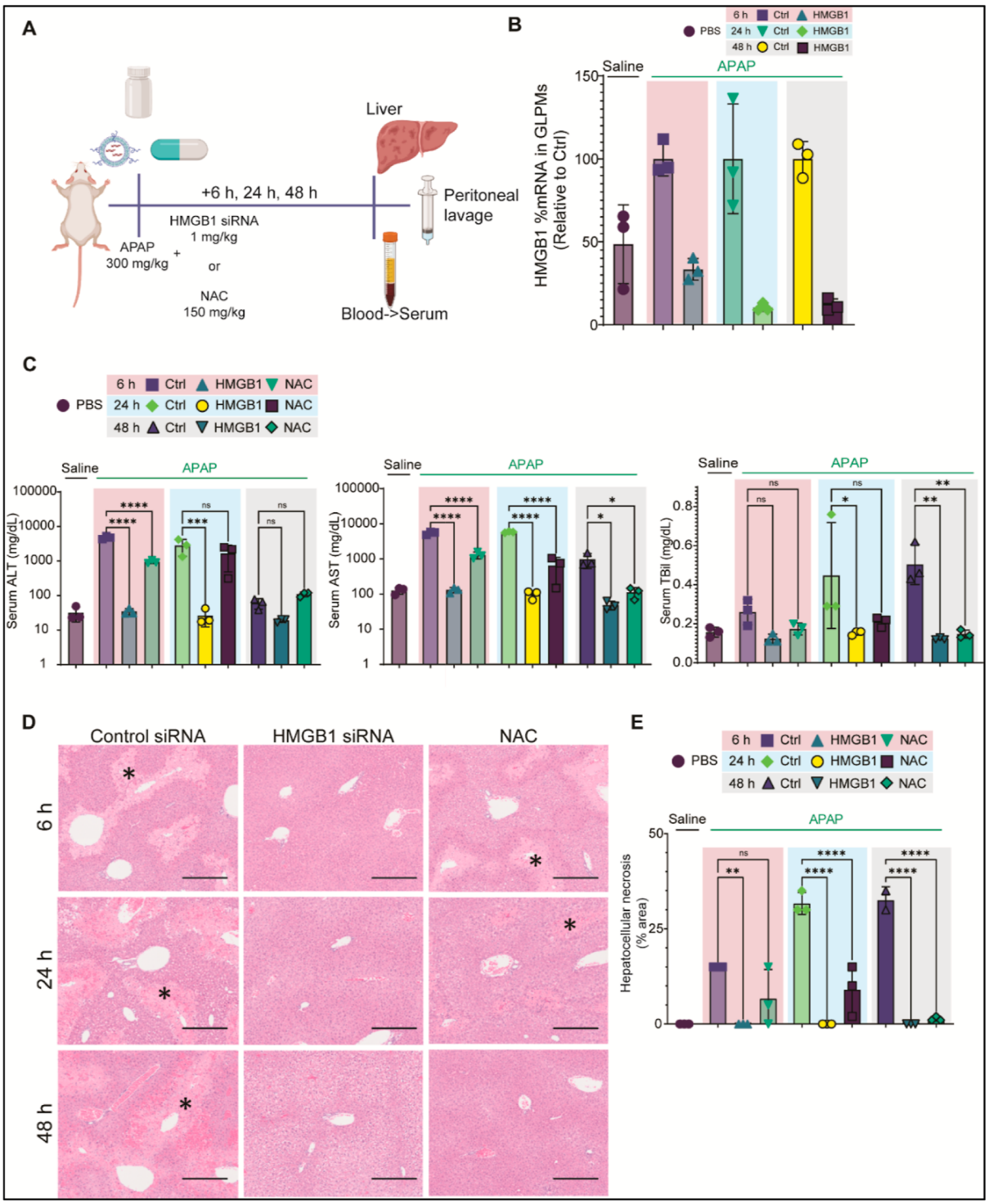

Figure 6. siRNA-mediated silencing of *HMGB1* in GLPMs renders a robust protection from APAP-induced hepatotoxicity in mice. (A) Study schematics and (B) relative mRNA expression of HMGB1 depicted as percentage mRNA remaining relative to expression in gLuc (control) siRNA at 6, 24, and 48 h post siRNA-Cy5 (C12−200) administration in both GLPMs and liver. mRNA expression was derived from qPCR after normalizing expression with an average of housekeeping genes PPIA and GAPDH. $n = 3$ for all groups. (C) Serum ALT (depicted on a log10 scale), serum AST (depicted on a $\log^{10}$ scale), and serum TBil in pg/mL for the respective treatment groups. (D) Representative histopathological images of liver H & E staining for the respective treatment groups. Hepatocellular degeneration/necrosis in centrilobular regions was seen in the gLuc (control) siRNA *at all time points* and NAC at 6 and 24 h post-APAP treatment (asterisks). Scale: 100 μm. Minimal/no degeneration was seen in the livers of the HMGB1 siRNA-treated group at all time points. Saline-treated control livers are not shown here. (E) Quantification of hepatocellular necrosis based on the histopathological scoring depicted as the percentage area of necrosis from the total field observed for the respective treatment groups. $n = 3$ for all groups. Data have been represented as mean ± SD. *$p < 0.05$, **$p < 0.01$, ***$p < 0.001$, ****$p < 0.0001$, ns not significant. P values were calculated with an ordinary one-way ANOVA followed by Dunnett's multiple comparison test, with a single pooled variance.

https://doi.org/10.1021/acsnano.4c18345
ACS Nano 2025, 19, 12102−12118

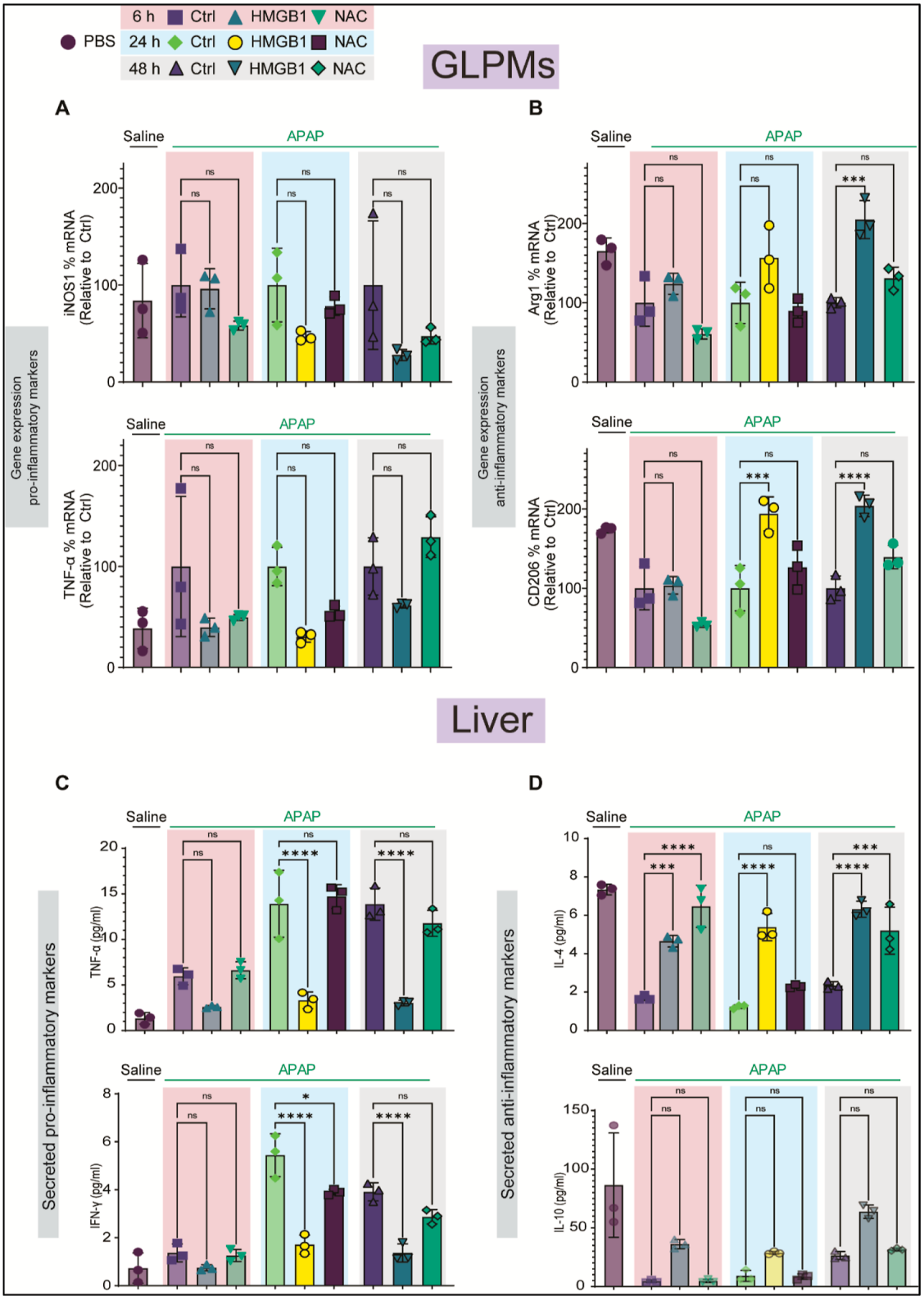

Figure 7. ***HMGB1*** **silencing in GLPMs prevents macrophage activation and protection of sterile liver injury caused by downstream inflammation by APAP-induced hepatotoxicity. (A) Relative mRNA expression of iNOS1 and TNF-α and (B) Arg1 and IL-10 in HMGB1 siRNA- and NAC-treated groups relative to expression in the gLuc (control) siRNA-treated group in GLPMs. (C) Secreted pro-inflammatory cytokine levels of TNF-α and IFN-γ in pg/mL in liver NPCs. (D) Secreted anti-inflammatory cytokine levels of IL-4 and IL-10 in pg/mL. $n = 4$ for all groups in liver NPCs. $N = 3$ for all groups. Data have been represented as mean $\pm$ SD. *$p < 0.05$, **$p < 0.01$, ***$p < 0.001$, ****$p < 0.0001$, ns not significant. *P* values were calculated with an ordinary one-way ANOVA followed by Dunnett's multiple comparison test, with a single pooled variance.**

https://doi.org/10.1021/acsnano.4c18345
ACS Nano 2025, 19, 12102−12118

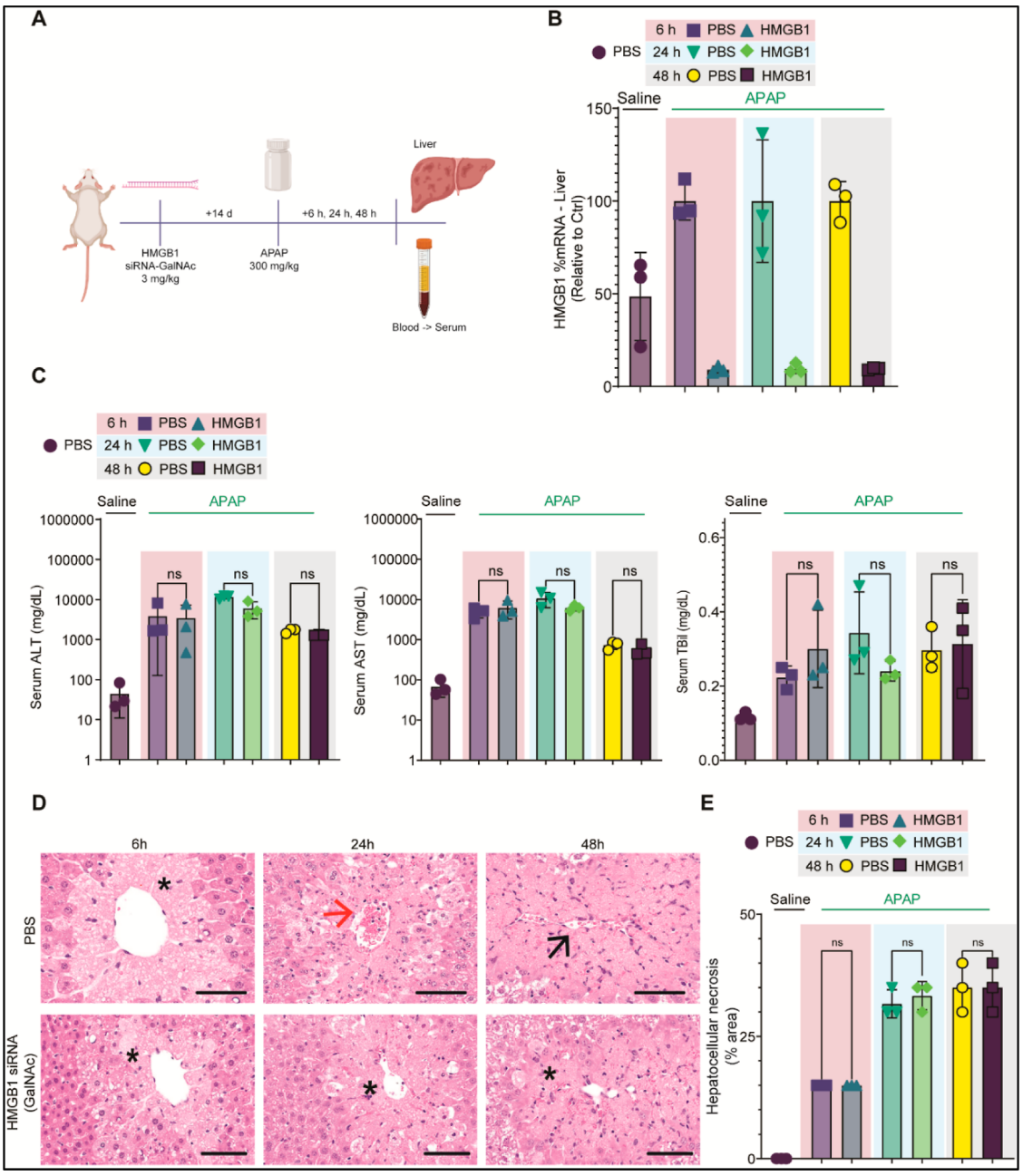

Figure 8. Silencing *HMGB1* in hepatocyte by GalNAc-conjugated siRNA does not lead to any protection from acute liver injury. (A) Study schematics and (B) relative mRNA expression of HMGB1 depicted as percentage mRNA remaining relative to expression in PBS control at 6, 24, and 48 h post siRNA-GalNAc administration in whole liver. The mRNA expression was derived from qPCR after normalizing expression with an average of housekeeping genes PPIA and GAPDH. $n = 3$ for all groups. (C) Serum ALT (depicted on a $\log^{10}$ scale), serum AST (depicted on a $\log^{10}$ scale), and serum TBil in pg/mL for the respective treatment groups. (D) Representative histopathological images of liver H & E staining for the respective treatment groups. Hepatocellular degeneration/necrosis in centrilobular regions was seen in the PBS (control) as well as the *HMGB1* siRNA-GalNAc-treated groups *at all time points* (asterisks) Scale: 50 μm. (E) Quantification of hepatocellular necrosis based on the histopathological scoring depicted as the percentage area of necrosis from the total field observed for the respective treatment groups. $n = 3$ for all groups. Data have been represented as mean ± SD. *$p < 0.05$, **$p < 0.01$, ***$p < 0.001$, ****$p < 0.0001$, ns not significant. *P* values were calculated with an ordinary one-way ANOVA followed by Dunnett's multiple comparison test, with a single pooled variance.

treatment (Figure 6E), albeit not as much as *HMGB1* siRNA-treatment, especially at the earlier 6 and 24 h time points.

***HMGB1* Silencing in GLPMs Prevents Macrophage Activation and Protects against Downstream Inflammation in AILI.** A significant reduction in pro-inflammatory macrophage markers i-NOS1 and TNF-α as well as normalization in the expression of anti-inflammatory markers Arg1 and CD206 was seen in the *HMGB1* siRNA-treated groups when compared to the gLuc control siRNA-treated groups (Figure 7A,B). Similarly, in liver, there were reductions in secreted pro-inflammatory cytokines TNF-α and IFN-γ as well as a normalization of anti-inflammatory cytokines IL-4 and IL-10 upon HMGB1 siRNA treatment when compared to the gLuc control siRNA-treated groups (Figure 7C,D) (Figure S10A,B).

NAC-treated groups also minimally impacted the macrophage inflammatory state with slightly lower iNOS1 expression

https://doi.org/10.1021/acsnano.4c18345
ACS Nano 2025, 19, 12102−12118

compared to gLuc siRNA and a mild reduction in liver inflammatory cytokines TNF-α and IFN-γ as well as some normalization of anti-inflammatory cytokine IL-4 (Figure 7A–D). Hence, by preventing the release of HMGB1 from the GLPMs, we could prevent macrophage modulation and, in turn, prevent liver injury by delivery of these siRNA-carrying GLPMs to the injured livers.

Direct *HMGB1* Silencing in Hepatocytes by GalNAc-Conjugated siRNA Does Not Protect against AILI. Since C12–200-based LNPs also led to functional gene silencing in the liver by 24 h, it was important to confirm whether the prevention of liver inflammation was due to silencing of HMGB1 in the migrating GLPMs or in the liver. To validate this, the same HMGB1 siRNA sequence was conjugated to a hepatocyte-specific *N*-acetyl galactosamine (GalNAc) ligand and tested in the mouse APAP injury model.[36] Upon siRNA-mediated silencing of hepatocyte-specific HMGB1 dosed at 3 mg/kg 14 days prior to APAP-administration, both serum chemistry and histopathological findings revealed that there was seemingly no protection to liver injury with similar levels of liver circulating injury markers as well as hepatocellular necrosis compared to the control-treated group when HMGB1 was silenced in hepatocytes (Figure 8A–E).

Based on the fast onset of action of siRNA-Cy5 (C12–200) targeting HMGB1 in GLPMs already by 6 h and their rapid migration to the injured liver and a nearly complete protection from injury as well as an anti-inflammatory phenotype as seen from markers as early as 6 h, this could be the primary initial mechanism of achieving protection of liver injury from the massive downstream inflammation propagated by APAP-driven liver injury and highlights the important translational potential of utilizing these siRNA-carrying GLPMS as delivery carriers of functional RNAi therapeutics to injured tissues, especially in more acutely driven injuries.

DISCUSSION

GATA6-expressing LPMs have known tissue-specific roles, and it has been established that they are unique in their ability to migrate to areas of injury within the peritoneum, a phenomenon not seen with other TRMs.[1,2,4−9] Our findings imply that this could be an inherent property of this mature innate immune cell population as they are readily available to sense injury in nearby tissues and can migrate and influence the microenvironment and the reparative ability of the injured tissue. With our studies, we achieved functional delivery of siRNAs to GLPMs residing in the peritoneal cavity by utilizing a C12-200-containing LNP and subsequently highlighted the potential therapeutic value of utilizing a cationic lipid moiety like C12-200 for delivering an RNAi therapeutic to an important TRM population like GLPMs. Not only that, but we further harnessed GLPM migration to an acutely injured liver driven by AILI, by utilizing them as functional RNAi delivery carriers to the injured liver and preventing liver injury and inflammation by silencing a prominent pro-inflammatory DAMP HMGB1. These findings were further solidified by the fact that silencing *HMGB1* by GalNAc-conjugated-siRNA within the liver did not lead to any meaningful benefit. Moreover, NAC, which is a clinically validated antidote for APAP-induced hepatotoxicity showed a relatively smaller and delayed benefit compared to silencing *HMGB1* in the GLPMs.[35]

Our results also shed light on the possibility of a TRM population like GLPMs intravasating into systemic circulation and migrating to the liver upon liver injury by APAP. We achieved this by tracking the migration of fluorophore-labeled macrophages in real-time by utilizing an innovative live-cell tracking method, DiFC, and then confirming findings by more traditional techniques of flow cytometry and IF in whole blood. This is different from what has been previously known about GLPMs taking an avascular route to rapidly infiltrate the liver upon eliciting a thermal probe-induced injury on the liver surface.[4] This shows that the migratory property and route of GLPM migration might be context-dependent on the type and region of liver injury.

Cues of large macrophage migration may lie in studying and comparing their behavior with tumor cell migration and metastasis as there may be similar pathways/mechanisms involved.[37−39] Although one of our study limitations was that it remains to be delineated as to understanding the mechanistic aspects of this migratory property, this opens an exciting scope of potentially utilizing them for a multitude of applications. Among the many directions that this work broadens, identifying specific mechanisms of intravasation and probing the liver microenvironment for specific factors/cytokines that signal the GLPMs to migrate and rapidly infiltrate the injured liver seem like some fascinating and important questions that we would be interested in addressing with future studies.

What has also been an equally intriguing question is whether we can utilize RNAi delivery to GLPMs to modulate macrophage polarization and use their migratory ability as targeted therapy. Our findings perhaps are closest to addressing this question and demonstrate that this seemingly naturally occurring phenomenon can be harnessed therapeutically by re-engineering GLPMs through RNAi-induced gene silencing simply by using an LNP delivery vector delivered in vivo and subsequently using them to influence the surrounding micro-environment of an injured tissue. Also, recently, other independent findings have also demonstrated similar localization of liposome-carrying infiltrating cells of myeloid origin to injured tissue in mice.[40] Additionally, our findings translate to a meaningful benefit in mitigating acute liver injury by modulation of macrophage polarization in AILI, which in the clinical setting, is still a huge health economics burden and leads to high mortality due to fulminant liver failure triggered by massive inflammation.[28,29]

Finally, it would be quite exciting to see the translatability of this phenomenon to higher species. Although our studies did not directly involve working on human samples, considering the evolutionarily conserved nature of these GLPMs in terms of location, phenotype, and function across species, it would be reasonable to expect a similar migration pattern in humans, especially in the context of acute injuries.[5] This broadens the scope to potentially develop RNAi and other possible gene modulation therapies targeted to GLPMs and envisions a future where they can be used as cell therapies without the need to draw them out and engineer them ex vivo. We hope that our work builds the foundation of advancing macrophage-delivery of oligonucleotides and other modalities and improves the landscape of macrophage-targeted therapies in the future.

CONCLUSIONS

Our study demonstrates the therapeutic potential of a GLPM-selective siRNA (C12–200) modality in AILI. RNAi-mediated silencing of a pro-inflammatory DAMP HMGB1 in liver infiltrating GLPMs upon acute liver injury mitigates the liver injury phenotype in mice. This therapeutically harnesses the unique migratory property of a TRM population like GLPM in

https://doi.org/10.1021/acsnano.4c18345
ACS Nano 2025, 19, 12102−12118

the context of a more physiologically relevant acute injury model. Overall, our approach showcases the ability to utilize these macrophages themselves as delivery carriers of LNP-carrying siRNAs to the injured liver, offering an efficient and effective option to expand the horizon of targeting macrophages as disease-modifying treatments.

EXPERIMENTAL METHODS

***In Vivo* Studies.** All investigations in live mice were carried out in accordance with the Institutional Animal Care and Use Committee (IACUC) at Northeastern University and Alnylam Pharmaceuticals and conformed to the NIH guidelines for the care and use of laboratory animals. Female BALB/c 8−12 week-old mice obtained from Charles River Laboratories were used for all the in vivo studies. Animals were maintained in a specific pathogen-free environment with ad libitum access to food and water, unless mentioned otherwise. Mice were housed under standardized conditions of temperature (21:22 °C) and illumination (12/12 h light/dark cycle).

APAP-Induced Hepatotoxicity Studies. For all the studies where APAP-induced hepatotoxicity was induced, mice were fasted overnight. This was done to deplete the glutathione reserves and lead to a more uniform injury caused by an overdose of APAP.[31] After an overnight fast, 300 mg/kg of APAP was dosed intraperitoneally (dose was never exceeded beyond this to comply with the Alnylam IACUC requirements), and food hoppers were replaced for ad libitum access to food. Water access was maintained throughout. At the end of the respective time points, the blood, peritoneal lavage, and liver were harvested. The retro-orbital (RO) route was employed to collect blood. Individual figures show specific study schematics. Depending on the downstream application, liver and blood were processed accordingly with details mentioned in respective sections.

For DiFC Studies. All the DiFC studies were carried out in the same manner as previously described.[10,17] Mice were anaesthetized with 2% isoflurane to reduce motion and kept under nosecone anesthesia to achieve a steady state of anesthesia. After shaving off the tail hair, optical fiber probes were then placed on the surface of the tail's vascular bundle along with ultrasound gel to minimize the index of refraction mismatch. Heating pads were used to preserve blood circulation to the extremities. Mice were scanned for 45 min, which, based on the flow rate of the tail vasculature, allowed us to interrogate the whole peripheral blood volume of the mouse several times.

Synthesis of siRNA Duplexes. All the siRNA synthesis was carried out exactly as previously described.[10] Double-stranded siRNA targeting HMGB1, NF-κB1, TLR4, and gLuc (control) were synthesized at and provided by Alnylam Pharmaceuticals (Table S3). Standard phosphoramidite chemistry was used for siRNA synthesis. Chemical modifications were applied to the siRNA template, as seen in Figure S6A, following same procedure as previously seen.[10,32,33] Deprotection and purification of the crude oligoribonucleotides by anion exchange high-performance liquid chromatography were carried out according to established procedures. Double-stranded siRNAs were then generated by annealing equimolar amounts of complementary sense and antisense strands.[10,22,32] A Cy5 fluorophore was labeled on the 5′-end of the sense strand before formulating the siRNA into LNPs. NM_001313894.1, NM_021297.3, and NM_008689.3 were utilized as the mRNA transcript reference sequences for HMGB1, TLR4, and NF-κB1, respectively, to design siRNAs against these targets. For the gLuc siRNA, *Gaussia princeps* luciferase mRNA was used to design siRNA (Accession #AY015993.1). For the HMGB1 siRNA sequence that was conjugated with a GalNAc-ligand, a trivalent GalNAc ligand was synthesized, and siRNA sequence targeting HMGB1 was then conjugated to the 3′-end of the sense strand as previously described.[33]

Formulation of C12-200-Based LNPs and siRNA-Cy5 Encapsulation. All the C12-200-based LNPs were prepared exactly as previously described.[10] Briefly, C12−200, 1,2-distearoyl-snglycero-3-phosphocholine (DSPC), cholesterol, and polyethylene glycol dimyristoyl glycerol (PEG-DMG) were dissolved in ethanol and mixed at a molar ratio of 50/10/38.5/1.5. The lipid solution was mixed with aqueous buffer containing siRNA-Cy5 via microfluidic mixing at a 1:3 ratio (Precision Nano systems, NanoAssemblr Benchtop Instrument); hence, an N/P ratio of 3 was used. The ethanol was then removed via buffer exchange in phosphate buffered saline (PBS, pH 7.2) by using dialysis. The particle size was determined using a Malvern Zetasizer NanoZS (Malvern, UK). Total siRNA-Cy5 content was determined by ion exchange high-performance liquid chromatography (Agilent) using a DNAPac PA200 column (Dionex Corporation Dionex, 260 nm, 55 °C run at 2 mL/min). Encapsulation efficiency was determined by the Quant-iT RiboGreen RNA assay (Invitrogen) and entrapment was determined by comparing the signal of the RNA-binding dye RiboGreen in formulation samples in the absence and presence of detergent Triton-X100 (2%). siRNA-Cy5 formulation characterization has been shown in Table S2.

DiFC Study Analysis. All the DiFC study analyses were carried out exactly as previously described.[10,17] Data generated by DiFC represent voltage (nA) over time (s). Photomultiplier tubes convert and amplify fluorescence generated from the siRNA-Cy5 (C12-200) carrying cells into current. After preprocessing data by subtracting background noise, we calculated the noise, which we define as the standard deviation of the data. Detections that were shown to have intensity spikes of at least five times greater than the calculated noise were referred to as "peaks". To reduce artifacts caused by motion or instrument noise, we employed a "matching" algorithm. This consists of analyzing the peak's height and width and matching it with similar peaks appearing in the second probe. When DiFC detects a peak in one optical fiber probe and then a following peak is detected in the other probe, separated by a predetermined time, we call this a "matched peak" since we can deduce that this is a cell traveling in either the arterial blood (from the heart to periphery) or the venous blood (from periphery to the heart). In this study, we present the mean peak count rates and mean peak amplitudes of only the "Fiber 1" probe for simplicity in data interpretation, but a similar matched "Fiber 2" data was also obtained (Figure S3).

Peritoneal Lavage Isolation and GLPM Enrichment. Peritoneal lavage was harvested from mice exactly as previously described and GLPMs were enriched following the steps in the peritoneal macrophage isolation kit from Miltenyi (kit details in Table S1) based on the principle of magnetic labeling and depletion of nonmacrophage cells from the isolated peritoneal lavage.[31] The enriched pool of mature macrophages was washed in ice cold PBS and resuspended in ACK lysis buffer to lyse red blood cells and resuspended back in 1× sterile PBS.

***In Vitro* Studies in GLPMs.** GLPMs were isolated and plated as previously described.[34] After isolation of primary mouse GLPMs as described above, cells were plated and cultured in a 6-well plate at a density of 2×10^6 cells/well in mouse peritoneal macrophage media (reagent details in Table S1). These cells were incubated in a 37 °C, 5% CO_2 cell culture incubator overnight.

siRNA-Cy5 (C12−200) Transfection. The following morning, cells were transfected with the respective siRNA-Cy5-(C12−200) formulations for 24 h at a dose of 100 nM of siRNA per well, and the cells were then harvested for RNA extraction and qPCR analysis of gene expression.

LPS *In Vitro* Studies. In all the LPS-macrophage activation studies, following overnight primary GLPM incubation, cells were coadministered with 100 μg/mL of LPS dissolved in 1× PBS along with siRNA-Cy5 (C12−200) treatment for 24 h.

Liver NPC Isolation. For all the experiments involving liver NPC isolation, following mouse euthanasia by CO_2 asphyxiation, livers were perfused via the portal vein, and NPCs were further isolated using mouse liver dissociation kit from Miltenyi Biotec following the kit manufacturer's protocol. Isolated NPCs were made into single cell suspensions that were later used for either flow cytometry or IF staining. Kit information is found in Table S1.

PBMC Isolation. PBMCs were collected exactly as previously described.[10] Studies where PBMCs were isolated, mice were put under anesthesia under 5% isoflurane, and blood was harvested by RO bleeds. This was followed by increasing the isoflurane in the chamber until induction of respiratory depression followed by puncturing the diaphragm following the IACUC guidelines. Blood was collected in K2 EDTA tubes to avoid any clotting, and 1 mL of ACK lysis buffer was added per 100 μL of whole blood and washed a couple of times. This

https://doi.org/10.1021/acsnano.4c18345
ACS Nano 2025, 19, 12102−12118

step was repeated, until the layer of RBCs was not seen. This was followed by washing with ice-cold sterile 1× PBS, making the PBMCs ready to be further prepared for flow cytometry staining and analysis.

Flow Cytometry Analysis. Single cell suspension was generated by pressing with a plunger of a 5 mL syringe through a 70 μm nylon mesh filter into a 50 mL conical tube and washing the cells through with 5−10 mL of PBS/FCS buffer. Finally, the cells were washed in cold sterile PBS, and resuspended in FACS buffer (eBioscience Flow Cytometry Staining Buffer, 00-4222-57). 50 μL amount of cell suspension (equivalent to 105 cells) was aliquoted in wells of a sterile 96-well U-bottomed plate and mixed gently by pipetting. This was followed by an addition of 50 μL of Fc block (anti-CD16/CD32 #BE0307; 2.4G2 clone; Bio X Cell, diluted 1−2:200, 0.5−1 μg) and incubated for 5−10 min to eliminate all nonspecific binding. Optimal concentration was predetermined for each antibody by prior run pilot studies. Desired antibodies were diluted to 2× the desired final concentration (1:200) in 100 μL of FACS buffer and added to the cell suspension, previously added to the respective wells (final Ab dilution 1:100). This was incubated for 20 min at 40 °C in the dark, followed by washes in sterile PBS, and finally, resuspended in 100 μL of FACS buffer and ran on the BD FACSymphony A3 Flow cytometer (BD Biosciences). Later, all the data generated on the flow cytometer were analyzed using the FlowJo v10.8 Software (BD Life Sciences). All the flow cytometry analysis was carried out after running compensation to adjust for any fluorophore wavelength overlap, as well as pregating all the live events, as well as singlets before proceeding. Detailed information on all the antibodies can be found in Table S1.

Histopathological Assessment and IHC Staining. Upon necropsy, livers were washed in ice-cold 1× PBS and the left-lateral lobe of the liver was transferred to a formalin containing jar for fixation, to be further processed into paraffin-embedded tissue blocks for immunohistochemical staining. All of the histopathology experiments were carried out by the Alnylam histopathology core group. The formalin containing left lobes of the livers was allowed to be fixed for 24 h and then placed onboard the Tissue-Tek VIP (Sakura) for automated processing. Samples were dehydrated in ethanol solutions of increasing concentrations until absolute ethanol, followed by tissue clearing by immersion in xylene with heat and vacuum pressure. The tissue sample was then impregnated with paraffin wax at 56 °C, embedded in a mold, and allowed to solidify. Paraffin blocks were sectioned at 4 μm slice thickness and placed on a water bath briefly before mounting on a charged glass slide.

H & E Staining. 4 μm tissue sections were stained onboard the Tissue Tek Prisma (Sakura), using a regressive protocol as follows: after dewaxing with xylene and rehydration to water, samples were stained with hematoxylin (Gills Hematoxylin II, Ricca) for 10 min and washed in distilled water followed by differentiation in an acid-alcohol solution (Nu-Clear, Epredia) dehydration to ethanol and then immersion in 0.5% eosin (Rubens Eosin-Phloxine, Biocare Medical) for 2 min followed by a quick water wash for 1 min. Slides then were dehydrated to xylene through a series of graded alcohols, as previously described, and coverslipped with a nonaqueous mounting medium.

GATA6 IHC. 4 μm tissue sections were stained onboard a Ventana Discovery Ultra (Roche). Unless otherwise specified, reagents are all manufactured by Roche for this instrument. The sections were stained using a standard immunohistochemistry procedure as follows: after dewaxing, slides underwent target retrieval in a 95 °C EDTA-based solution for 1 h, followed by a general block (Background Sniper, Biocare Medical) and peroxidase inhibitor before the application of the primary antibody (Gata6, Cell Signaling #5851S) at a 1:50 dilution for 1 h. After primary antibody incubation, an antirabbit secondary was applied for 30 min, followed by DAB chromogen development, then hematoxylin counterstaining, and bluing. Finally, slides were taken off the autostainer, dehydrated to xylene through a series of graded alcohols, and covered with a nonaqueous mounting medium.

Serum Chemistry. Additionally, blood samples were collected in the serum separator tubes by RO bleeding and were processed into serum by centrifuging them at 10,000*g* for 10 min at 40 °C and removal of supernatant serum samples to fresh protease/nuclease free tubes. Serum samples were run into a Beckman Coulter/Olympus AU480 clinical analyzer (Olympus, AU480) to measure some liver injury enzymes like serum ALT, AST, and liver function biomarker like total bilirubin as per the manufacturer's instructions.

Relative Gene Expression Quantification by qPCR. RNA from the respective tissue or cell matrix (liver, liver NPCs, GLPMs) was isolated using the Qiagen 96w tissue extraction kit (74181). A NanoDrop 8000 Spectrophotometer was used to measure the RNA concentration. All RNA samples were diluted to 10 ng/μL in RNase-free water, from which 50 μL was used for complementary DNA (cDNA) synthesis using the Applied Biosystems High-Capacity cDNA Reverse Transcription Kit with the RNase Inhibitor. For qPCR reactions, 2 μL of ≤20 ng of cDNA was used. RT qPCR was performed using the LightCycler 480 Probes Master in the LightCycler 480 real-time qPCR system. Commercially available mouse TaqMan primers and probes were used for RT-qPCR analysis. Each sample was analyzed in duplicate by RT-qPCR. The *Cq* values for all samples were calculated by using LightCycler software. Replicate *Cq* values for each individual animal at each time point for measured gene or housekeeping genes were averaged. The 2 ΔCq was calculated for each animal at each time point, where ΔCq was calculated by subtracting the average of the geo-mean of replicate housekeeping sample from the average replicate measured gene *Cq* per sample. The resultant delta−delta threshold Cycle (relative quantification) [$\Delta\Delta Cq$(RQ)] values obtained for measured mRNA relative to the average of housekeeping genes PPIA and GAPDH mRNA from individual animals were used to quantify the fold change of treated samples relative. Detailed assay ID for all Taqman assays are shown in Table S1.

Secreted Cytokine Quantification by ELISA. We utilized the Luminex Cytokine & Chemokine 36-Plex Mouse ProcartaPlex (Thermo Fisher) kit to quantify the levels of 36 well characterized secreted cytokines and chemokines from both the isolated liver NPCs as well as peritoneal lavage supernatant after GLPM enrichment.

IF Staining. IF staining was carried out as previously described.[10] Once the single cell suspension was isolated either from whole PBMCs or liver NPCs, cells were cultured in low-glucose DMEM containing 2% FBS and 1% penicillin/streptomycin at a concentration of 5×10^4 cells per well in a 96-well tissue-culture treated plate (cell carrier-96 ultra, 6055300) and left in an incubator (5% CO_2, 37 °C) overnight. Cell media was removed, and 50 μL of fixative (4% PFA in PBS) (paraformaldehyde solution, 4% in PBS, Thermo Scientific) was added to each well. After an incubation of 10 min at room temperature (RT), fixative was removed and cells were washed with ice cold PBS (3×). Cells were then incubated in 50 μL per well of PTX permeabilization buffer (0.3% TritonX-100 in PBS) (diluted from Triton X-100, Sigma-Aldrich, 9036-19-5) for 10 min at RT and again washed with ice cold PBS (3×) thereafter. Cells were then blocked in a blocking buffer (5% NGS in PBS + 0.1% Tween-20) for 1 h at RT in the dark. After aspirating the blocking solution, 50 μL per well of the respective primary antibody solutions were added. Primary antibody solutions were prepared by diluting Abs in PBST (PBS + 0.1% Tween-20) (information on primary Abs used described in Table S1). Cells were incubated at 40 °C overnight in the dark, followed by washes with ice cold PBST (3×), addition of 50 μL of the respective secondary antibody solution (diluted in PBST similarly), and incubation for 2 h at RT in the dark. After aspiration of secondary antibody, cells were washed 2× in ice cold PBST, and during the last wash, NucBlue Live ReadyProbes Reagent (Hoechst 33342) was added, and cells were incubated for 5 min. This was aspirated, and cold PBS was added, followed by sealing the plate. The plate was analyzed on an Opera Phenix High Content confocal microscope from PerkinElmer. Digital images were acquired using a 20× objective lens, and quantification of imaged cells was carried out by the automated algorithms of the confocal microscope after optimization and background subtractions.

Statistical Analysis. All data are expressed as mean ± SD. Statistical significance was determined by either unpaired Student *t*-test (two-tailed) whenever comparison between two groups was involved. In the case of 3 or more groups, one way-ANOVA (two-tailed), followed by Tukey's post hoc test was used to determine statistical significance. All the experimental findings were reproduced with biological replicates of 4 unless specified otherwise, and individual

https://doi.org/10.1021/acsnano.4c18345
ACS Nano 2025, 19, 12102−12118

experiments were reproduced twice to confirm the consistency of results. A p-value of <0.05 was considered statistically significant. All the statistical analysis was carried out using GraphPad Prism v7.01 (GraphPad by Dotmatics, 2022 GraphPad Software). For all the figures, *p < 0.05, **p < 0.01, ***p < 0.001, ****p < 0.0001, ns not significant.

ASSOCIATED CONTENT

Supporting Information

The Supporting Information is available free of charge at https://pubs.acs.org/doi/10.1021/acsnano.4c18345.

Figures incorporating additional information about the siRNAs used and in vitro characterization in the primary mouse GLPMs to demonstrate the silencing of respective target genes, IF and immunohistopathological images to give deeper insights into the migratory ability of GLPMs to the liver upon AILI, along with a more detailed characterization of a panel of pro-inflammatory cytokines within the LPMs and liver, detailed schematics to better enable interpreting DiFC data along with the overall model of mechanism of all the experimental studies, some additional flow cytometry details including gating strategies, and a detailed list of all the reagents and materials used along with detailed formulation characteristics and encapsulation efficiency of C12-200-loaded siRNAs (PDF)

Raw data for the relevant figures (XLSX)

AUTHOR INFORMATION

Corresponding Author

Mansoor M. Amiji − *Department of Pharmaceutical Sciences, School of Pharmacy and Pharmaceutical Sciences, Northeastern University, Boston, Massachusetts 02115, United States; Department of Chemical Engineering, College of Engineering, Northeastern University, Boston, Massachusetts 02115, United States;* orcid.org/0000-0001-6170-881X; Phone: 617-373-3137; Email: m.amiji@northeastern.edu

Authors

Dhaval Oza − *Department of Pharmaceutical Sciences, School of Pharmacy and Pharmaceutical Sciences, Northeastern University, Boston, Massachusetts 02115, United States; Alnylam Pharmaceuticals, Cambridge, Massachusetts 02142, United States*

Fernando Ivich − *Department of Bioengineering, College of Engineering, Northeastern University, Boston, Massachusetts 02115, United States*

Kirsten Deprey − *Alnylam Pharmaceuticals, Cambridge, Massachusetts 02142, United States*

Kelsey Bittner − *Alnylam Pharmaceuticals, Cambridge, Massachusetts 02142, United States*

Keith Bailey − *Alnylam Pharmaceuticals, Cambridge, Massachusetts 02142, United States*

Sarah Goldman − *Alnylam Pharmaceuticals, Cambridge, Massachusetts 02142, United States*

Mikyung Yu − *Alnylam Pharmaceuticals, Cambridge, Massachusetts 02142, United States*

Mark Niedre − *Department of Bioengineering, College of Engineering, Northeastern University, Boston, Massachusetts 02115, United States*

Ho-Chou Tu − *Alnylam Pharmaceuticals, Cambridge, Massachusetts 02142, United States*

Complete contact information is available at: https://pubs.acs.org/10.1021/acsnano.4c18345

Author Contributions

Conceptualization: DO, MA, HCT, MN. Methodology: DO, FI (for DiFC studies), KD (flow cytometry), KB, KB (immunohistochemistry), SG (siRNA synthesis), MY (LNP formulation). Investigation: DO. Visualization: DO. Funding acquisition: MA, Alnylam Pharmaceuticals. Project administration: DO, MA. Supervision: MA, HCT, MN. Writing—original draft: DO, MA. Writing—review and editing: DO, MA, FI.

Funding

This study was supported by Alnylam Pharmaceuticals through the Industrial PhD program administered by Northeastern University.

Notes

The authors declare no competing financial interest.

ACKNOWLEDGMENTS

We would like to start by thanking the entire Alnylam Pharmaceuticals Research Department, with a special shout-out to the medium-scale synthesis team, for their constant support with all the siRNA synthesis. Special thanks to A. Rogers, Y.A. Rodriguez, W. Cantley, L. Noetzli, L. Bondurant, J. Farley, and K. Yucius for providing intellectual and experimental design inputs with some of the studies. Some of the experimental design schematics as well as the table of contents graphics were generated using BioRender.com. We also wanted to thank F. Tremblay for providing vital initial intellectual input and a big thanks to K. Fitzgerald for providing the constant support that we needed to carry out this important work. Lastly, we wanted to thank S. Gordon for his feedback, guidance, and mentorship throughout.

REFERENCES

(1) Oza, D.; Amiji, M. M. In *Macrophage Targeted Delivery Systems: Basic Concepts and Therapeutic Applications*; Gupta, S., Pathak, Y. V., Eds.; Springer International Publishing, 2022; pp 357−378.

(2) Zhao, J.; Andreev, I.; Silva, H. M. Resident tissue macrophages: Key coordinators of tissue homeostasis beyond immunity. *Sci. Immunol.* **2024**, *9*, No. eadd1967.

(3) Parayath, N. N.; Parikh, A.; Amiji, M. M. Repolarization of Tumor-Associated Macrophages in a Genetically Engineered Nonsmall Cell Lung Cancer Model by Intraperitoneal Administration of Hyaluronic Acid-Based Nanoparticles Encapsulating MicroRNA-125b. *Nano Lett.* **2018**, *18*, 3571−3579.

(4) Wang, J.; Kubes, P. A Reservoir of Mature Cavity Macrophages that Can. Rapidly Invade Visceral Organs to Affect Tissue Repair. *Cell* **2016**, *165*, 668−678.

(5) Salm, L.; Shim, R.; Noskovicova, N.; Kubes, P. Gata6(+) large peritoneal macrophages: an evolutionarily conserved sentinel and effector system for infection and injury. *Trends Immunol.* **2023**, *44*, 129−145.

(6) Okabe, Y.; Medzhitov, R. Tissue-specific signals control reversible program of localization and functional polarization of macrophages. *Cell* **2014**, *157*, 832−844.

(7) Majeske, A. J.; Bayne, C. J.; Smith, L. C. Aggregation of sea urchin phagocytes is augmented in vitro by lipopolysaccharide. *PLoS One* **2013**, *8*, No. e61419.

(8) Honda, M.; Kadohisa, M.; Yoshii, D.; Komohara, Y.; Hibi, T. Directly recruited GATA6 + peritoneal cavity macrophages contribute to the repair of intestinal serosal injury. *Nat. Commun.* **2021**, *12*, 7294.

(9) Zindel, J.; Peiseler, M.; Hossain, M.; Deppermann, C.; Lee, W. Y.; Haenni, B.; Zuber, B.; Deniset, J. F.; Surewaard, B. G. J.; Candinas, D.; et al. Primordial GATA6 macrophages function as extravascular platelets in sterile injury. *Science* **2021**, *371*, No. eabe0595.

(10) Oza, D.; et al. Lipid nanoparticle encapsulated large peritoneal macrophages migrate to the lungs via the systemic circulation in a model of clodronate-mediated lung-resident macrophage depletion. *Theranostics* **2024**, *14*, 2526−2543.
(11) Lazarov, T.; Juarez-Carreño, S.; Cox, N.; Geissmann, F. Physiology and diseases of tissue-resident macrophages. *Nature* **2023**, *618*, 698−707.
(12) Ardura, J. A.; Rackov, G.; Izquierdo, E.; Alonso, V.; Gortazar, A. R.; Escribese, M. M. Targeting Macrophages: Friends or Foes in Disease? *Front. Pharmacol* **2019**, *10*, 1255.
(13) Murray, P. J. Macrophage Polarization. *Annu. Rev. Physiol.* **2017**, *79*, 541−566.
(14) Woolbright, B. L.; Jaeschke, H. Role of the inflammasome in acetaminophen-induced liver injury and acute liver failure. *J. Hepatol.* **2017**, *66*, 836−848.
(15) Ivich, F.; Calderon, I.; Fang, Q.; Clark, H.; Niedre, M. Ratiometric fluorescence sensing and quantification of circulating blood sodium sensors in mice in vivo. *Biomed. Opt. Express* **2023**, *14*, 5555−5568.
(16) Ivich, F.; Pace, J.; Williams, A. L.; Shumel, M.; Fang, Q.; Niedre, M. Signal and measurement considerations for human translation of diffuse in vivo flow cytometry. *J. Biomed. Opt.* **2022**, *27*, 067001.
(17) Tan, X.; Patil, R.; Bartosik, P.; Runnels, J. M.; Lin, C. P.; Niedre, M. In Vivo Flow Cytometry of Extremely Rare Circulating Cells. *Sci. Rep.* **2019**, *9*, 3366.
(18) Pace, J.; Ivich, F.; Marple, E.; Niedre, M. Near-infrared diffuse in vivo flow cytometry. *J. Biomed. Opt.* **2022**, *27*, 097002.
(19) Wei, P.-S.; et al. Enhancing RNA-lipid nanoparticle delivery: Organ- and cell-specificity and barcoding strategies. *J. Controlled Release* **2024**, *375*, 366−388.
(20) Love, K. T.; et al. Lipid-like materials for low-dose, in vivo gene silencing. *Proc. Natl. Acad. Sci. U.S.A.* **2010**, *107*, 1864−1869.
(21) Novobrantseva, T. I.; et al. Systemic RNAi-mediated Gene Silencing in Nonhuman Primate and Rodent Myeloid Cells. *Mol. Ther. Nucleic Acids* **2012**, *1*, No. e4.
(22) Chen, R.; Kang, R.; Tang, D. The mechanism of HMGB1 secretion and release. *Exp. Mol. Med.* **2022**, *54*, 91−102.
(23) Pisetsky, D. S.; Jiang, W. Role of Toll-like Receptors in HMGB1 Release from Macrophages. *Ann. N.Y. Acad. Sci.* **2007**, *1109*, 58−65.
(24) Yuan, J.; Guo, L.; Ma, J.; Zhang, H.; Xiao, M.; Li, N.; Gong, H.; Yan, M. HMGB1 as an extracellular pro-inflammatory cytokine: Implications for drug-induced organic damage. *Cell Biol. Toxicol.* **2024**, *40*, 55.
(25) Shang, J.; Zhao, F.; Cao, Y.; Ping, F.; Wang, W.; Li, Y. HMGB1 mediates lipopolysaccharide-induced macrophage autophagy and pyroptosis. *BMC Mol. Cell Biol.* **2023**, *24*, 2.
(26) Yang, R.; Tonnesseen, T. I. DAMPs and sterile inflammation in drug hepatotoxicity. *Hepatol. Int.* **2019**, *13*, 42−50.
(27) Yamamoto, T.; Tajima, Y. HMGB1 is a promising therapeutic target for acute liver failure. *Expet Rev. Gastroenterol. Hepatol.* **2017**, *11*, 673−682.
(28) Bower, W. A.; Johns, M.; Margolis, H. S.; Williams, I. T.; Bell, B. P. Population-based surveillance for acute liver failure. *Am. J. Gastroenterol.* **2007**, *102*, 2459−2463.
(29) Bernal, W.; Wendon, J. Acute liver failure. *N. Engl. J. Med.* **2013**, *369*, 2525−2534.
(30) Lotze, M. T.; Tracey, K. J. High-mobility group box 1 protein (HMGB1): nuclear weapon in the immune arsenal. *Nat. Rev. Immunol.* **2005**, *5*, 331−342.
(31) Bianchi, M. G.; et al. Titanium dioxide nanoparticles enhance macrophage activation by LPS through a TLR4-dependent intracellular pathway. *Toxicol. Res.* **2015**, *4*, 385−398.
(32) Ganbold, T.; Bao, Q.; Zandan, J.; Hasi, A.; Baigude, H. Modulation of Microglia Polarization through Silencing of NF-κB p65 by Functionalized Curdlan Nanoparticle-Mediated RNAi. *ACS Appl. Mater. Interfaces* **2020**, *12*, 11363−11374.
(33) Brown, C. R.; et al. Investigating the pharmacodynamic durability of GalNAc-siRNA conjugates. *Nucleic Acids Res.* **2020**, *48*, 11827−11844.
(34) Rietschel, E. T.; et al. Bacterial endotoxin: molecular relationships of structure to activity and function. *FASEB J.* **1994**, *8*, 217−225.
(35) James, L. P.; McCullough, S. S.; Lamps, L. W.; Hinson, J. A. Effect of N-acetylcysteine on acetaminophen toxicity in mice: relationship to reactive nitrogen and cytokine formation. *Toxicol. Sci.* **2003**, *75*, 458−467.
(36) Rajeev, K. G.; et al. Hepatocyte-Specific Delivery of siRNAs Conjugated to Novel Non-nucleosidic Trivalent N-Acetylgalactosamine Elicits Robust Gene Silencing in Vivo. *ChemBioChem* **2015**, *16*, 903−908.
(37) Sznurkowska, M. K.; Aceto, N. The gate to metastasis: key players in cancer cell intravasation. *FASEB J.* **2022**, *289*, 4336−4354.
(38) Wong, S. Y.; Hynes, R. O. Lymphatic or hematogenous dissemination: how does a metastatic tumor cell decide? *Cell Cycle* **2006**, *5*, 812−817.
(39) Chiang, S. P.; Cabrera, R. M.; Segall, J. E. Tumor cell intravasation. *Am. J. Physiol. Cell Physiol.* **2016**, *311*, C1−c14.
(40) Deprez, J.; et al. Transport by circulating myeloid cells drives liposomal accumulation in inflamed synovium. *Nat. Nanotechnol.* **2023**, *18*, 1341−1350.

https://doi.org/10.1021/acsnano.4c18345
ACS Nano 2025, 19, 12102−12118